

# DuDoSS: Deep-Learning-Based Dual-Domain Sinogram Synthesis

## from Sparsely Sampled Projections of Cardiac SPECT

### Supplementary Materials

Xiongchao Chen<sup>1</sup>, Bo Zhou<sup>1</sup>, Huidong Xie<sup>1</sup>, Tianshun Miao<sup>1,2</sup>, Hui Liu<sup>2</sup>, Wolfgang Holler<sup>4</sup>, MingDe Lin<sup>2,5</sup>, Edward J. Miller<sup>2,3</sup>, Richard E. Carson<sup>1,2</sup>, Albert J. Sinusas<sup>1,2,3</sup>, Chi Liu<sup>1,2</sup>

<sup>1</sup>Department of Biomedical Engineering, Yale University, New Haven, Connecticut, United States, 06511

<sup>2</sup>Department of Radiology and Biomedical Imaging, Yale University, New Haven, Connecticut, United States, 06511

<sup>3</sup>Department of Internal Medicine (Cardiology), Yale University School of Medicine, New Haven, Connecticut, United States, 06511

<sup>4</sup>Visage Imaging GmbH, Berlin, Germany, 12163

<sup>5</sup>Visage Imaging, Inc., San Diego, California, United States, 92130

#### Running Title

DUAL SINOGRAM SYNTHESIS of CARDIAC SPECT

#### Correspondence

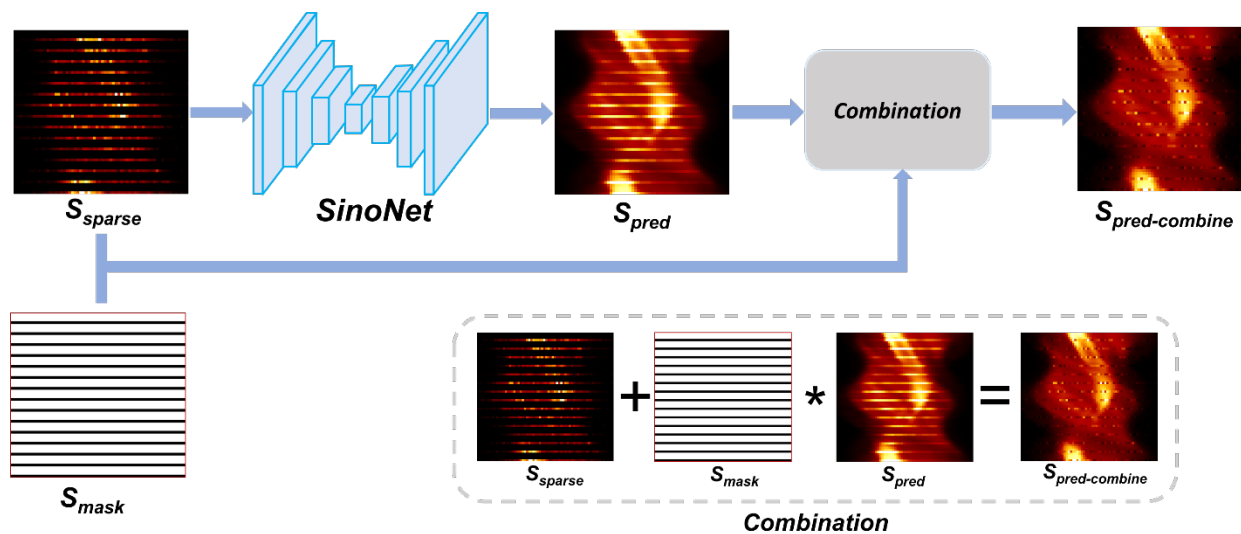
Chi Liu, Department of Radiology and Biomedical Imaging, Department of Biomedical Engineering, Yale University, New Haven, CT, 06511. Email: [chi.liu@yale.edu](mailto:chi.liu@yale.edu)

#### Acknowledgements

This work is supported by NIH grant R01HL154345.

25 **Section 1. Schematics of Direct Sino2Sino and Direct Img2Img**

26



27

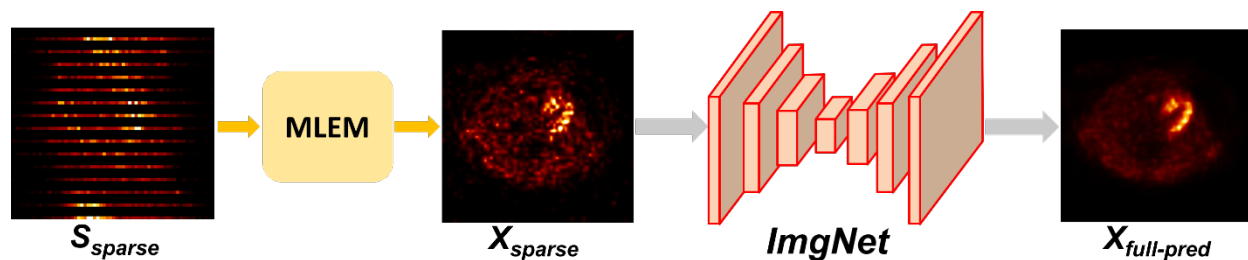
28

29

30

31

**FIGURE S-1.** Schematics of Direct Sino2Sino.



32

33

34

35

**FIGURE S-2.** Schematics of Direct Img2Img.

36

37

38

39

40

The schematic of Direct Sino2Sino was shown in Figure S-1. The Direct Sino2Sino was implemented only in the sinogram domain. The zero-padded sparse-view projections  $S_{sparse}$  were input to the SinoNet to predict the synthetic full-view projections  $S_{pred}$ , with the ground-truth full-view projections  $S_{full}$  as targets. Then, Angle 1 of  $S_{pred}$  was replaced by ground-truth Angle 1 in a combination module to produce  $S_{pred-combine}$  for the reconstruction of the predicted full-view SPECT image.

41

42

43

44

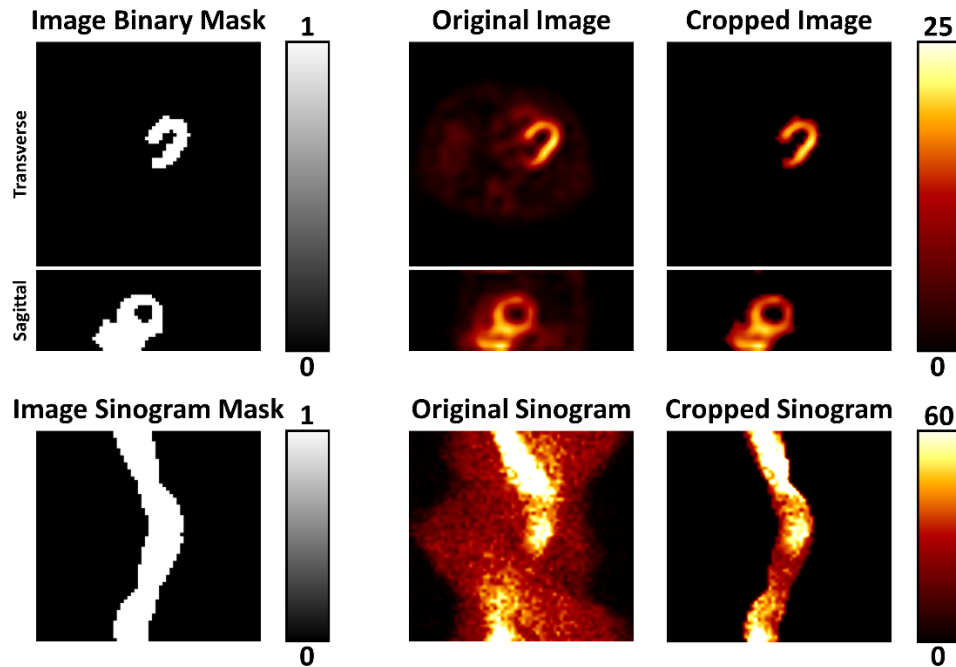
45

46

The schematic of Direct Img2Img was shown in Figure S-2. Direct Img2Img was implemented only in the image domain, without any intermedia step of synthetic projections. The SPECT image  $X_{sparse}$  reconstructed using  $S_{sparse}$  was input to the ImgNet to directly generate the predicted full-view image  $X_{full-pred}$ , with the ground-truth full-view image  $X_{full}$  as targets.

## 47 Section 2. Binary masks for quantitative evaluations of images and sinograms

48 Figure S-3 shows the sample binary masks for quantitative evaluations of images and sinograms. The  
 49 binary image masks were generated by voxel thresholding to restrict quantitative evaluations within the  
 50 voxels of the patient heart. Then, we applied forward projection to the binary image masks to generate the  
 51 binary sinogram masks to restrict the quantitative evaluations within the cardiac sinogram regions. The  
 52 images or sinograms were element-wise multiplied with the binary image or sinogram masks before the  
 53 quantitative evaluations based on NMSE/NMAE/PSNR/SSIM.



54  
 55  
 56

FIGURE S-3. Binary image and sinogram masks, original and cropped images and sinograms.

### 57 Section 3. Synthetic projections by DuDoSS by different loss functions

58 Table S-1 shows the quantitative evaluations of the synthetic sinograms by DuDoSS supervised by  
 59 different combinations of loss functions, including L1, L2, SSIM, and KL-divergence loss. It can be  
 60 observed that the DuDoSS groups using other loss functions including L2, SSIM, and KL-divergence  
 61 generate either similar ( $p > 0.05$ ) or inferior performance ( $p < 0.001$ ) compared to that using L1 loss. Thus,  
 62 L1 loss function is currently the most simple but effective loss function in this sinogram synthesis study.

63

64 Table S-1. Voxel-wise quantitative evaluations of the synthetic projections using different loss functions on  
 65 DuDoSS. The best results are marked with **bold**.

Testing Loss Functions	NMSE ( $\times 10^{-2}$ )	NMAE ( $\times 10^{-2}$ )	SSIM	PSNR	P-value <sup>a</sup>
Loss: L1 <sup>b</sup> (proposed)	<b>1.65 <math>\pm</math> 0.72</b>	<b>8.95 <math>\pm</math> 1.56</b>	<b>0.9842 <math>\pm</math> 0.0067</b>	<b>37.09 <math>\pm</math> 4.51</b>	–
Loss: L1 + SSIM <sup>c</sup>	1.67 $\pm$ 0.73	8.98 $\pm$ 1.55	0.9842 $\pm$ 0.0066	37.04 $\pm$ 4.46	0.124
Loss: L1+KL <sup>d</sup>	1.68 $\pm$ 0.75	8.99 $\pm$ 1.58	0.9842 $\pm$ 0.0066	37.02 $\pm$ 4.46	< 0.001*
Loss: L2	1.69 $\pm$ 0.76	9.02 $\pm$ 1.58	0.9840 $\pm$ 0.0069	37.00 $\pm$ 4.39	< 0.001*
Loss: L2 + SSIM	1.70 $\pm$ 0.80	9.05 $\pm$ 1.63	0.9839 $\pm$ 0.0069	36.99 $\pm$ 4.36	< 0.001*

66 <sup>a</sup>Two-tailed paired t-test of NMSE between the current and L1 loss group in the table.

67 <sup>b</sup>L1 loss function.

68 <sup>c</sup>Structural similarity loss function.

69 <sup>d</sup>KL-divergence loss function.

70 \*Refers to significant difference with a significance level of 0.05.

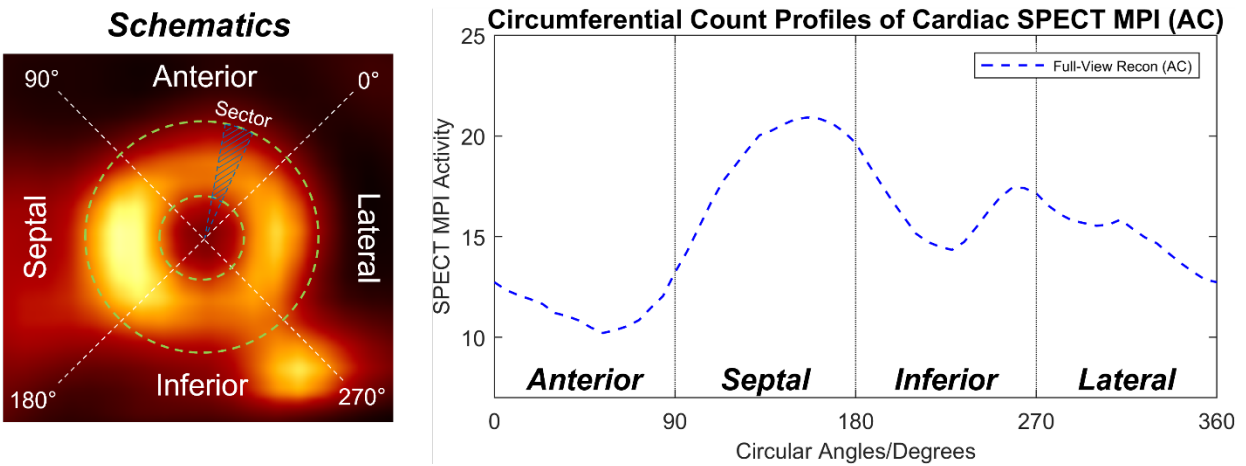
71

72

## 73 Section 4. Implementations of the short-axis circumferential profiles

74 Figure S-4 shows the short-axis (SA) circumferential count profiles of cardiac myocardial perfusion  
 75 imaging (MPI). In this figure, the circular cardiac myocardial perfusions are evenly divided into 90 sectors  
 76 with 4 degrees for each sector, which is shown in the schematics at the bottom left. The averaged intensities  
 77 of the sectors along the anterior, septal, inferior, and lateral were computed and plotted as the figure at the  
 78 bottom right.

79



80

81 **FIGURE S-4.** Short-axis Circumferential Count Profiles in short-axis view of Cardiac SPECT  
 82 myocardial perfusion imaging.

83

84